Structural and optical properties of Eu^{3+} doped Y_2O_3 nanostructures embedded in amorphous alumina waveguides prepared by pulsed laser deposition

2006 J. Phys.: Condens. Matter 18 10043

(http://iopscience.iop.org/0953-8984/18/44/005)

INSTITUTE OF PHYSICS PUBLISHING JOURNAL OF PHYSICS: CONDENSED MATTER

J. Phys.: Condens. Matter **18** (2006) 10043–10058 doi:10.1088/0953-8984/18/44/005

Structural and optical properties of Eu^{3+} doped Y_2O_3 nanostructures embedded in amorphous alumina waveguides prepared by pulsed laser deposition

A Pillonnet[1,5], J Lancok[1,2], C Martinet[1], O Marty[3], J Bellessa[4] and C Garapon[1]

[1] Laboratoire de Physico-Chimie des Matériaux Luminescents, UMR CNRS 5620, UCB Lyon I, 10 rue André-Marie Ampère, 69622 Villeurbanne Cedex, France
[2] Institute of Physics, Academy of Science of the Czech Republic, Na Slovance, 182 21 Prague, Czech Republic
[3] Laboratoire d'Electronique, Nanotechnologies et Capteurs, EA CNRS 3780, UCB Lyon I, France
[4] Laboratoire de Physique de la Matière Condensée et Nanostructures, UMR CNRS 5586, UCB Lyon I, France

E-mail: annep@pcml.univ-lyon1.fr

Received 28 July 2006, in final form 2 October 2006
Published 20 October 2006
Online at stacks.iop.org/JPhysCM/18/10043

Abstract

Composite optical waveguides of Eu doped Y_2O_3 nanolayers with various theoretical thicknesses from 10 to 0.2 nm embedded in an amorphous alumina matrix were prepared by targeted alternating pulsed laser ablation. Their structural and fluorescence properties were compared to those of thick nanocrystallized Eu:Y_2O_3 films deposited under the same conditions. Whereas layers with thicknesses of 5 and 10 nm are continuous and crystalline, layers with thickness of less than 2 nm are constituted of isolated amorphous nanoparticles with a mean height of around 1 nm, according to transmission electron microscopy and atomic force microscopy. The Eu^{3+} fluorescence properties show that Eu^{3+} ions are localized in different sites inside the nanolayers or nanoparticles or at the interface with the matrix, depending on the size of the nanostructure. The refractive index of the composite waveguides was measured by m-line spectroscopy. Waveguiding propagation was observed.

1. Introduction

Sesquioxides, such as Y_2O_3, Gd_2O_3 and Lu_2O_3, are well-known and efficient host matrices for rare earth ions for luminescence applications. In recent years interest has shifted towards luminescent rare-earth doped sesquioxide nanocrystals because of the observed modifications

[5] Author to whom any correspondence should be addressed.

of their spectroscopic properties as compared to those of bulk materials [1–5]. It appears that some changes are still quite controversial and depend strongly on the preparation method, which has an important influence on the surface states and the structural disorder. The modification of the fluorescence properties appears in particular for the spectral characteristics. Additional broadening or shifts of lines have been observed relative to the bulk crystals. They have been attributed to surface ions, which experience different environments from those of the particle core and whose contribution increases as the particle size decreases. For nanocrystals with sizes of less than about 6 nm, very broad spectra, similar to those of amorphous materials, could even be observed. The dynamic fluorescence properties also appear modified, due to an increased disorder or an increase in the concentration of defect quenching centres, which induce a lifetime shortening [2] as well as lower concentration quenching for nanocrystals [2, 6]. Finally a gap blue-shift was observed as for semiconducting nanocrystals [4].

When these sesquioxide nanocrystals are embedded in a dielectric amorphous waveguiding film they may give specific properties to the composite material, such as a high emission cross-section or low phonon energy, and thus induce new potentialities for practical application in integrated optics. In order to investigate the effects of nanoparticles size, structure and environment on their fluorescence properties, we have focused our attention on europium doped yttrium oxide nanoparticles and compared their properties when they form pure nanocrystalline thin films and when they are embedded in alumina in nanocomposite thin films. Several methods may be used to grow yttrium oxide nanocrystalline and nanocomposite thin films, but to grow the latter several steps are generally necessary. For example, nanoparticles, prepared by colloidal synthesis [5], were introduced into the sol, which is used afterwards for sol–gel preparation of waveguides by dip-coating [7]. Pulsed laser deposition (PLD) may successfully provide rare earth doped Y_2O_3 films, as well as epitaxial films for waveguides or phosphor applications [8, 9] or nanocrystallized waveguides [10] depending on the experimental conditions. Moreover, this method permitted us to prepare a composite material without any post-processing and with an efficient control of the structure dimension and topography by using alternating ablation of targets of the different film components. For example, deposition of oxide or metal nanoparticles included in an alumina matrix has been reported, the nanoparticle condensation being achieved in the plasma plume at high pressure or on the substrate at low pressure [11, 12].

This paper presents the preparation by PLD of waveguides consisting of Eu:Y_2O_3 nanostructures embedded in an amorphous alumina matrix. The appropriate experimental conditions for growing amorphous alumina and Eu:Y_2O_3 nanocrystals and their respective deposition rates were deduced from pure alumina and Eu:Y_2O_3 thick film deposition. Transmission electron microscopy was used to study the influence of the thickness of the deposited Y_2O_3 layers on their crystalline properties. Their growth mode was observed by atomic force microscopy for single layer deposition. Since Eu^{3+} ions are good structural probes, the study of their fluorescence properties permitted us to get further information on the structural properties of the nanostructures and to study the effects of their size, structure and interfaces with the matrix on both spectral and dynamic emission characteristics of the Eu^{3+} doping ions.

2. Experimental details

2.1. Pulsed laser deposition

The films were prepared using a Lambda-Physik LPX-100 KrF excimer laser ($\lambda = 248$ nm) at 10 Hz repetition rate and constant high voltage mode. The laser was focused on rotating targets to a 3 mm^2 spot and the laser beam energy density was adjusted between 0.5 and 3 J cm^{-2} by

means of an OPTEC 4020 attenuator. The targets consisted of Al_2O_3 or Eu:Y_2O_3 powders, with a 5% Eu/Y atomic ratio, which had been pressed and sintered at 1400 °C for 12 h in air. The target to substrate distance was 4 cm. Deposition were performed in an ultra-high-vacuum chamber (base pressure 10^{-6} Pa) at 1 or 10^{-2} Pa oxygen pressure. Depending on the analysis to be performed, films were deposited on fused silica or Pyrex substrates or on silicon wafers. The substrate surface temperature was adjust between room temperature and 730 °C by means of resistive heating. No *in situ* annealing was performed and sample cooling took place at the same pressure as that used during deposition.

The composite films were prepared by alternating ablation of two targets of Al_2O_3 and Eu:Y_2O_3. The laser pulse number used for the ablation of each target necessary to get a given thickness was deduced from the growth rates, which had been determined from the thicknesses of thick pure oxide films fabricated under the same conditions. Films with Eu:Y_2O_3 layers of various theoretical thicknesses (T_{theo}) were deposited. The synchronization of target choice and laser pulse number was computer controlled.

2.2. Structural and fluorescence analysis

The crystalline structure of the films was determined by x-ray diffraction (XRD) using a Siemens D500 diffractometer with Cu Kα radiation in the θ–2θ configuration. The crystallite sizes were deduced from XRD spectra using the Scherrer formula [13].

The structural and composition properties of the composite films were studied by transmission electron microscopy (TEM) with a Topcom EM-002B microscope, working at 200 kV and using Kevex Sigma energy dispersive x-ray equipment.

Investigation of the growth mode of Eu:Y_2O_3 layers on amorphous Al_2O_3 surfaces was done by atomic force microscopy (AFM) using a Topometrix explorer atomic force microscope in contact mode with SFM probes type 1520-00 and a 2 μm type scanner.

Accurate determination of thickness and refractive index of the films were achieved by m-line spectroscopy using an He–Ne laser beam at 543.5 nm, assuming a step index profile [14]. Propagation losses were estimated from the attenuation of the light scattered along the propagation path [15].

The fluorescence spectra were recorded at room temperature by two experimental systems. First, the emission and excitation spectra were performed using a 450 W Xe lamp as the excitation source. The excitation wavelength was selected by a H10D Jobin-Yvon monochromator with a band-pass of 8 nm [4]. The photoluminescence was collected by an optical fibre and analysed by a TRIAX 320 Jobin-Yvon monochromator and a Peltier cooled charge coupled device detector with a resolution of 0.5 nm. For excitation spectra, the emission signal was selected through the same monochromator with a 6 nm band-pass and detected by a photomultiplier and a photon counting system. Second, the emission spectra were realized at 308 nm excitation provided by a pulsed XeCl excimer laser source (LUMONICS). The fluorescence was analysed by a Hilger and Watts monochromator with a 0.8 nm resolution and registered through a cooled AsGa photomultiplier (RCA31084) by a photon counting system (Ortec) or a multichannel analyser (Canberra) for the decay registration.

3. Results and discussion

3.1. Growth conditions of nanocomposite films

As a first step, Eu^{3+} doped yttrium oxide and alumina films were prepared to determine the best temperature, oxygen pressure and laser fluence conditions to obtain, on the one hand,

Table 1. Deposition conditions (P, oxygen pressure; T_S, substrate temperature; F, fluence) and structural properties deduced from XRD of alumina and Eu:Y_2O_3 films.

Sample	Target	P (Pa)	T_S (°C)	F (J cm^{-2})	XRD
YOC	Eu:Y_2O_3	10^{-2}	730	0.5	Cubic $\varnothing = 52 \pm 3$ nm
YON	Eu:Y_2O_3	1	560	1	Cubic $\varnothing = 5 \pm 1$ nm
YOM	Eu:Y_2O_3	10^{-2}	640	3	Monoclinic $\varnothing = 40 \pm 3$ nm
YOA	Eu:Y_2O_3	1	20	2	Amorphous
AlO	Al_2O_3	1	560	3	Amorphous

nanosized cubic crystallites for Eu:Y_2O_3 and, on the other hand, an amorphous phase for alumina. The influence of the deposition parameters on the properties of yttrium oxide and alumina films has been described in previous papers [10, 16]. A compromise should be found between temperature, pressure and fluence [10]. For a given pressure, the temperature should be high enough to get crystalline cubic yttrium oxide but low enough to promote the growth of crystallites with small size with minimal diffusion, which could be detrimental in the case of multilayer structures. In addition, for a given temperature, the pressure should sufficiently high, because a pressure decrease induces the formation of the monoclinic phase, but not too high, so as to obtain an amorphous layer due to the decrease in the energy of the ablated species. Moreover, the fluence should be decreased in order to favour the cubic phase relative to the monoclinic one. For example, for a 730 °C substrate temperature, 10^{-2} Pa oxygen pressure and 0.5 J cm^{-2} fluence, a film labelled YOC, was grown with a cubic (111) oriented structure and 50 nm crystallite size [10], whereas at a 560 °C substrate temperature, 1 Pa oxygen pressure and 1 J cm^{-2}, a cubic Eu:Y_2O_3 film, labelled YON with (111) orientation and nanometric crystallite size of about 5–7 nm was formed. For the same deposition conditions, alumina films are amorphous [16]. In addition, a monoclinic film, labelled YOM, was deposited at 640 °C, 10^{-2} Pa and 3 J cm^{-2}, for fluorescence comparison. Table 1 summarizes the growth conditions and structural properties of the films presented in this paper.

The conditions, 560 °C, 1 Pa, 1 J cm^{-2}, were chosen to prepare the composite films of Eu doped Y_2O_3 nanolayers embedded in an amorphous Al_2O_3 matrix, whose structural and optical properties will be described in detail. The deposition always started with an alumina layer and a protective alumina layer was deposited at the end. Alternate ablation of Eu doped Y_2O_3 and alumina targets was done with laser pulse numbers on each target calculated in order to deposit a fixed theoretical thickness T_{theo} equal to 10 nm for the alumina layers (220 pulses) and various T_{theo} of 10, 5, 2, 1, 0.5 and 0.2 nm for the Eu:Y_2O_3 layers, which correspond to 200, 100, 40, 20, 10 and 4 pulses, respectively. For comparison, some single and multi-bilayers were deposited at 730 °C, 10^{-2} Pa and 0.5 J cm^{-2}.

3.2. Structural properties of nanocomposite films

According to XRD, all the composite films appear amorphous, as no diffraction lines could be detected, except for very broad ones, due to the amorphous alumina matrix or the silica substrate in the case of the thinnest films. They could, however, contain crystallites, which could not be detected by XRD, if they are too small or not numerous enough for the small amount of matter analysed in the $\theta/2\theta$ configuration.

The structural properties of the composite films, particularly the shape and the crystalline phase of the Eu:Y_2O_3 nanostructures inside the Al_2O_3 matrix, were then analysed by TEM on cross-section images obtained with cleaved samples. For this purpose, films with 10 Eu:Y_2O_3/Al_2O_3 bilayers containing Eu:Y_2O_3 layers with T_{theo} equal to 10, 5, 2, 1 and 0.2 nm

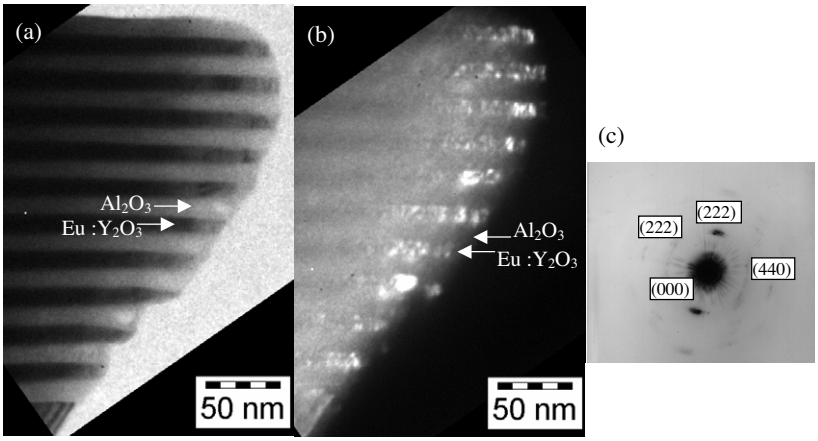

Figure 1. TEM bright (a) and dark (b) field images and electron diffraction pattern (c) of a cross-section of alternating Eu:Y_2O_3 and Al_2O_3 layers with 10 nm theoretical thickness.

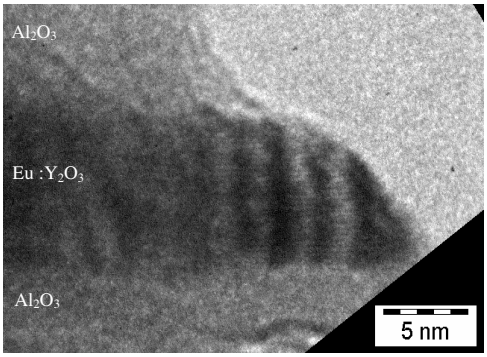

Figure 2. HRTEM image of alternating Eu:Y_2O_3 and Al_2O_3 layers with 10 nm theoretical thickness.

were deposited on thin (0.3 mm) Si substrates. Figure 1 shows the TEM bright field image of Eu:Y_2O_3/Al_2O_3 multilayers with Eu:Y_2O_3 thickness T_{theo} equal to 10 nm. A highly regular alternation of dark Eu:Y_2O_3 and bright Al_2O_3 layers is observed, the identification of Al and Y elements having been checked by Kevex Sigma energy dispersive x-ray spectroscopy. The layers appear as homogeneous, and their thickness T_{theo} is equal to 10 nm. From the electron diffraction of each layer type, the Al_2O_3 layers are amorphous whereas a cubic crystalline structure is found for the Eu:Y_2O_3 layers (figure 1(c)). The dark field image, realized by selecting one of the spots in this electron diffraction pattern, reveals that Eu:Y_2O_3 layers exist as cubic nanocrystallites, whose shape is elongated.

The HRTEM image (figure 2) shows, for the Eu:Y_2O_3 layers, a columnar growth with a (111) orientation of crystallites, having a height and width of about 8–10 nm and 2–3 nm, respectively. The (111) planes are clearly observed inside each column and an interplanar distance of 1.88 Å, close to the 1.874 Å value of cubic Y_2O_3, was measured.

The 5 nm thick layers grow with the same (111) oriented columnar cubic structure, the crystals having height of about 4–5 nm and width of 2–3 nm.

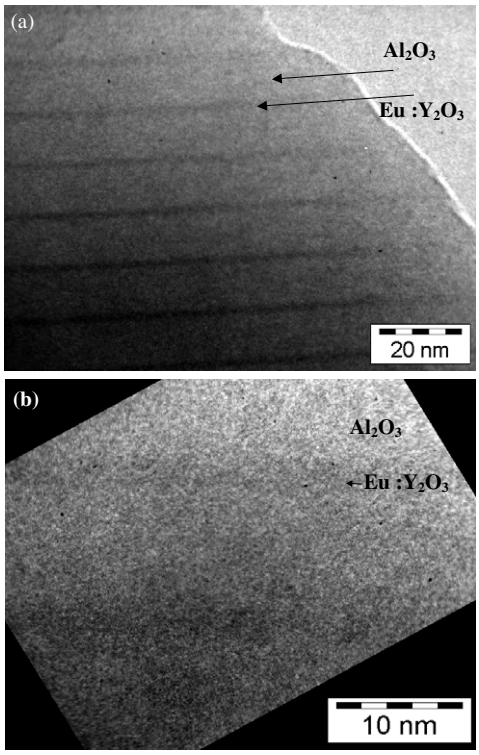

Figure 3. TEM bright field image (a) and HRTEM image (b) of Eu:Y_2O_3 and Al_2O_3 multilayers with 0.2 and 10 nm theoretical thickness, respectively.

No crystalline structure was observed for layers with a theoretical thickness lower than 2 nm. Figure 3 shows a TEM bright field image of Eu:Y_2O_3/Al_2O_3 multilayers with Eu:Y_2O_3 of theoretical thickness T_{theo} equal to 0.2 nm. The Al_2O_3 layers are homogeneous and their thickness corresponds to the theoretical 10 nm value. The contrast between Al_2O_3 layers and Eu:Y_2O_3 layers is not as good as in figure 1 and the measured thickness of Eu:Y_2O_3 layers (1.3 nm) is larger than the 0.2 nm theoretical thickness. The electron diffraction pattern and HRTEM images show that the Eu:Y_2O_3 layers are amorphous.

The crossover between amorphous and cubic phase is for T_{theo} of the order of 2 nm. However, it was observed that the Eu:Y_2O_3 nanostructures of theoretical thickness 2 or 1 nm, which are amorphous, could rather quickly crystallize in the cubic phase inside the microscope under the influence of the electron beam, within 10 and 30 min, respectively, whereas no crystallization took place for thinner layers. This suggests the existence of very small domains, with a local order similar to the cubic one, which could play the role of nucleation centres.

Moreover, the change in the structural properties of the Eu:Y_2O_3 layers around 2 nm is also detected by the ratio between their measured T_{meas} and theoretical T_{theo} thicknesses. For theoretical thicknesses of 10 and 5 nm, this ratio is equal to 1, which means that the layers are continuous. For theoretical thickness decreasing below 2 nm, the measured thickness is much higher than the expected value and the ratio $T_{\text{meas}}/T_{\text{theo}}$ tends to increase (figure 4). The reproducibility has been checked by the observation of different samples deposited under the same conditions. From this, we may conclude that the Eu:Y_2O_3/Al_2O_3 interface is becoming very rough and that the Eu:Y_2O_3 layers are not continuous but consist of isolated particles with

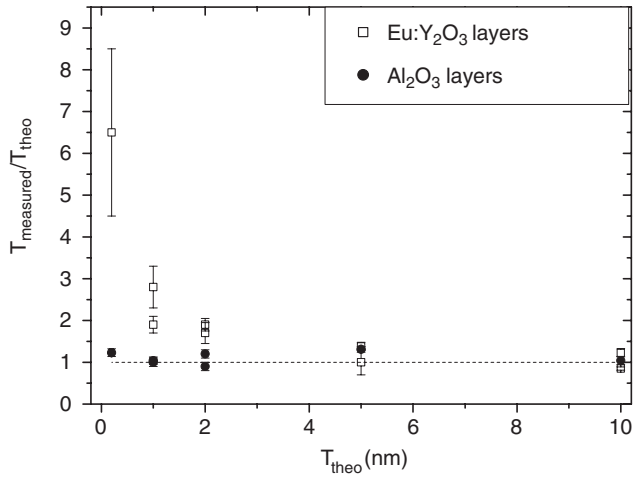

Figure 4. Ratio between the thickness measured by TEM and the theoretical thickness of the Eu:Y_2O_3 layers and alumina layers inside Eu:Y_2O_3/Al_2O_3 multilayers as a function of the theoretical thickness of the Eu:Y_2O_3 layers.

a height greater than the theoretical thickness. If the analysed section of the sample is not thin enough, as may be the case for the present samples, nanoparticles cannot be visualized separately and a continuous layer with a weak contrast and rough and shallow interfaces is observed.

3.3. AFM study of single Eu:Y_2O_3 nanolayers deposited on amorphous Al_2O_3 surfaces

In order to get further information on the growth process of Eu:Y_2O_3 layers in the composite films, we studied by AFM the morphology of single layers of Eu:Y_2O_3, with various thicknesses, deposited on an amorphous alumina surface. Pyrex substrates were used for this analysis because their rms roughness (0.2 nm) is less than that of fused silica or silicon substrates (0.6 nm), which makes observations easier and more reliable. The topographic images of three samples have been compared (figure 5). A 10 nm thick Eu:Y_2O_3 layer (figure 5(c)) appears as continuous and its rms roughness is quite similar to that of a 10 nm thick Al_2O_3 layer (figure 5(a)) or to that of the Pyrex substrate and is equal to 0.2 ± 0.1 nm.

On the contrary, the surface of a 1 nm thick Eu:Y_2O_3 layer on Al_2O_3 surface (figure 5(b)) appears to be constituted of isolated particles with polydisperse heights in the nanometre range. Image analysis provides the height distribution of these particles, which is presented in figure 6. The mean height of the particles corresponds to the lattice parameter of cubic Y_2O_3 (1.06 nm). This means that the majority of the particles are formed of one layer equivalent to the unit cell, which could correspond to a layer-by-layer growth regime. The presence of particles of greater height, however, suggests that some 3D nucleated growth also takes place. Although we need a more thorough investigation to determine the precise growth mode of Y_2O_3 nanostructures on an amorphous alumina layer, we deduce from these experiments that for an effective thickness below 2 nm Eu:Y_2O_3 isolated nanoparticles rather than continuous layers are deposited.

Our results have been compared with those of a study devoted to the structure of thin layers of Eu:Y_2O_3 epitaxially grown on single crystalline (100) α-Al_2O_3 substrates by the same PLD method [17]. AFM observations revealed that very smooth films are grown for thicknesses of the order of 1 nm, which indicates a layer-by-layer regime, and that island growth was observed

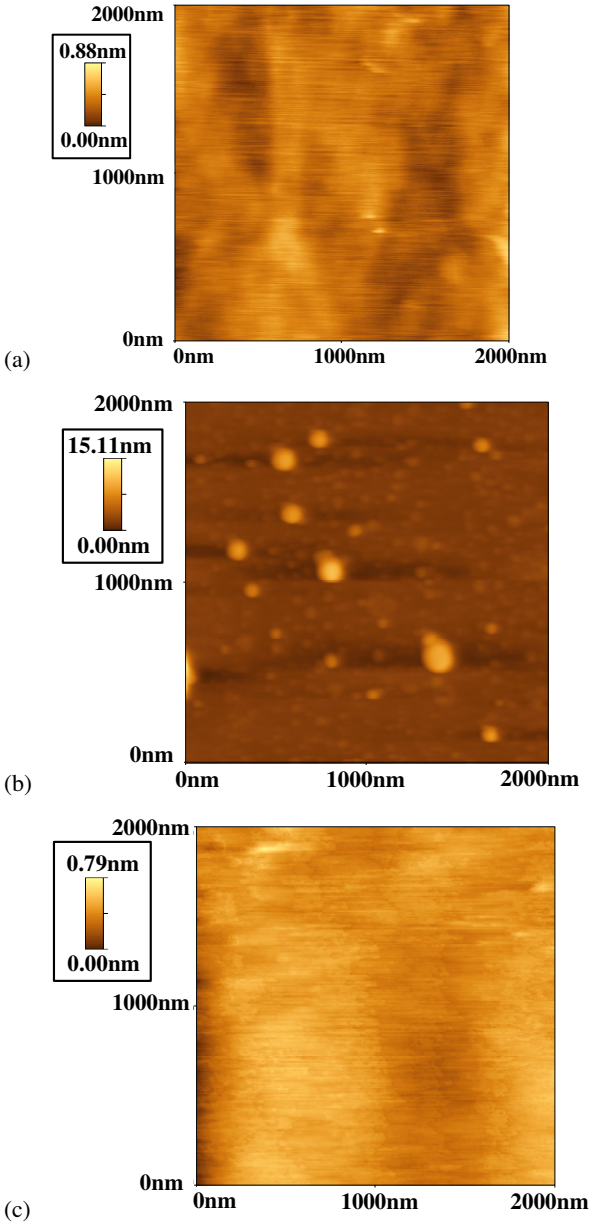

Figure 5. AFM images of surfaces of Al_2O_3 (T_{theo} = 10 nm) (a), Eu:Y_2O_3 (T_{theo} = 1 nm) on Al_2O_3 (T_{theo} = 10 nm) (b) and Eu:Y_2O_3 (T_{theo} = 10 nm) on Al_2O_3 (T_{theo} = 10 nm) (c) deposited on Pyrex substrates.

(This figure is in colour only in the electronic version)

for film thicknesses above about 4 nm. This result may appear to be in disagreement with our observations of a smooth surface for 10 nm thick layers and islands for 1 nm thick layers. This difference may be due to the higher deposition temperature (800 °C) which was used for the epitaxial growth and which should increase the surface mobility and favour 2D growth,

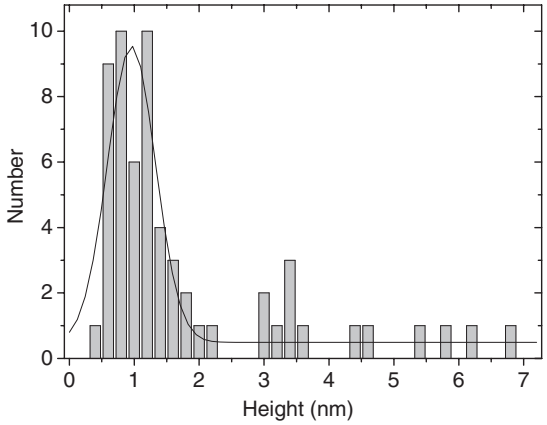

Figure 6. Distribution curve of height of Eu:Y_2O_3 particles determined by image analysis of figure 5(b).

whereas for the 560 °C temperature, which we used here, the limited mobility leads to isolated nanoparticles, for the same 1 nm theoretical thickness. For higher theoretical thicknesses, the epitaxial growth induces increasing roughness due to the stress relaxation mechanism leading to island growth, whereas in our case nanocrystallization extends, due to the amorphous substrate and lower temperature.

3.4. Fluorescence properties

3.4.1. Eu:Y_2O_3 nanocrystalline films. The Eu^{3+} emission spectra, in the $^5D_0 \rightarrow {}^7F_J$ transition range, restricted to the lowest multiplets $J = 0, 1, 2$, are presented in figure 7(a) for cubic Eu^{3+}:Y_2O_3 films with two different crystallite sizes, YOC and YON, and for the micrometre-sized cubic powder used for target preparation. In addition, the spectrum of the monoclinic YOM film is presented. The 308 nm excitation corresponds to an absorption into the $^5F_2$ multiplet of the f configuration. The spectra of all the cubic samples show the same lines, which are mainly due to Eu^{3+} ions located in the site of C_2 symmetry [18, 19], the lines due to the S_6 site being much weaker [20]. In particular, two characteristic $^5D_0 \rightarrow {}^7F_2$ lines of Eu^{3+} in cubic Y_2O_3 are located at 611 and 631 nm. The spectra of the nanocrystalline YON and YOC films, however, are broadened and show additional features, a shoulder located at about 613 nm, which broaden towards a longer wavelength as the crystallite size decreases, and a broad line centred at 624 nm. These additional features, whose intensity and width increase as the crystallite size decreases, are a clear indication that Eu^{3+} ions are distributed among sites of different crystal field symmetry and strength. By analogy with the conclusions of spectroscopic and EXAFS studies on nanocrystalline powders prepared by the combustion method [2, 21], they are attributed to Eu^{3+} ions located in a perturbed environment at the crystallite surfaces.

This fluorescence modification is, however, different from those observed for nanopowders prepared by sol-lyophilization [4], colloidal precipitation [5] or low energy cluster beam deposition [22], which emphasizes the crucial role of surface properties.

The question of whether these additional features located at wavelengths (614 and 624 nm) close to those (615 and 624 nm) of the main emission lines of the B and C sites of monoclinic Y_2O_3 [23] could be attributed to a parasitic monoclinic phase, which would not have been detected by XRD, should be discussed. Depending on the deposition parameters, films with mixed monoclinic and cubic phases may indeed be prepared by PLD [10]. In addition a cubic

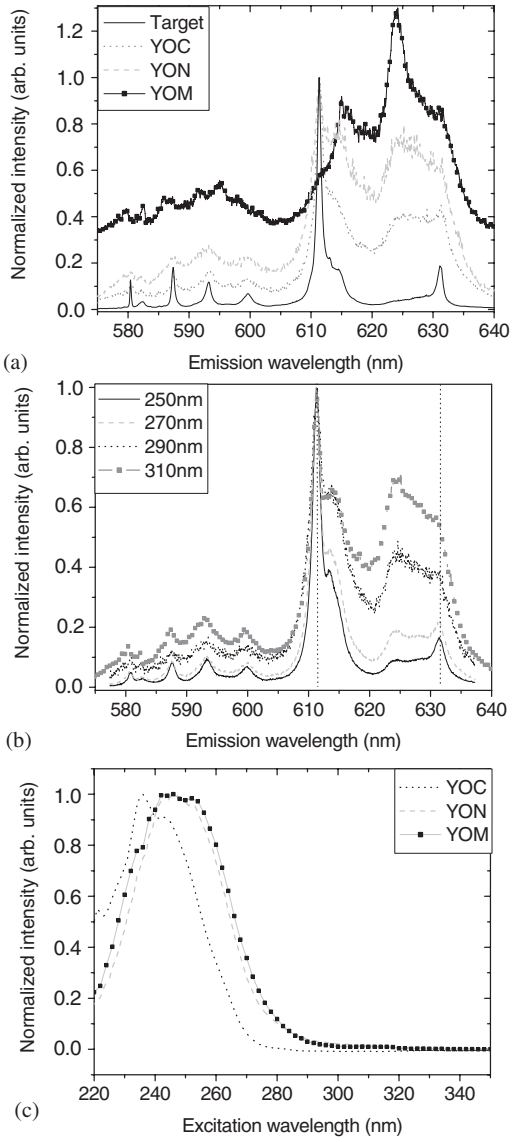

Figure 7. Emission spectra of the Eu doped Y_2O_3 target and YON, YOC and YOM films for $\lambda_{ex} = 308$ nm (a) and of YON film for $\lambda_{exc} = 250$, 270, 290, 310 nm (b). Excitation spectra of YOC and YON cubic films ($\lambda_{em} = 611 \pm 6$ nm) and of YOM monoclinic film ($\lambda_{em} = 615 \pm 6$ nm).

to monoclinic phase transformation was suggested for nanocrystals [24], although it appears that this effect does not depend just on the nanocrystal size but also on the details of sample synthesis and post-treatments [25]. In our case, we think that the contribution to the spectra of Eu^{3+} ions located in monoclinic crystals must be excluded because of a broader profile and the absence of the corresponding transitions in the $^5D_0 \rightarrow {}^7F_{0,1}$ transition range. The three lines of the $^5D_0 \rightarrow {}^7F_1$ transition remain at the same position (587.6, 593.3 and 600 nm) as for the cubic phase, although they get strongly broadened, without any marked line at 586, 592 or 595 nm, which would be due to the monoclinic phase. It cannot be excluded, however,

that the local environment of the perturbed surface Eu^{3+} ions could have some similarities with that experienced by Eu^{3+} ions in the B or C sites of the monoclinic phase, as these sites are characterized by a higher coordination number (7 instead of 6 for cubic sites) and a lower site symmetry than the perturbed sites, evidenced by EXAFS [21]. Further experiments with site-selective excitation into the $^5D_0$ level are under way to clarify this point.

Figure 7(b) shows the spectra of the cubic YON film, with the smallest crystallite size, obtained by excitation at various wavelengths into the charge transfer band (CT). This band originates from the interaction between Eu^{3+} and O^{2-} ions and is located at 239 nm for micrometre-sized crystals [2]. The emission spectra depend strongly on the excitation wavelength within the CT band. As the excitation wavelength increases, the relative intensity of the additional lines increases and all the lines broaden; in particular, the $^5D_0 \rightarrow {}^7F_0$ line becomes broader towards the high energy side.

This evolution is confirmed by the excitation spectra, which were recorded for the two nanocrystalline Eu:Y_2O_3 films, monitoring the 611 nm most intense emission line, with a band width of 6 nm which includes the additional 613 nm line (figure 7(c)). In addition, the excitation spectrum of the monoclinic YOM film, monitoring at 615 ± 6 nm emission wavelength, is presented. Whereas the CT band is observed at 239 nm for the YOC film with large crystallites, it is centred at 246 nm for the nanocrystalline YON film. As the size of cubic crystallites decreases, a red shift of the CT band is observed, which is due to an increased contribution of the perturbed ions emitting the additional 613 nm line. This result is in agreement with those reported for Eu:Y_2O_3 nanocrystalline powders prepared by the combustion method [2]. The red shift of the CT band was, in that case, attributed to an increase in coordination number from 6 to 8 and in the Eu–O bond length for Eu^{3+} ions located at the nanocrystallite surface [21]. A red shift of the CT band is also observed for the monoclinic YOM film compared with the cubic YOC film with a similar crystallite size, this could be attributed to the increase in coordination number from cubic to monoclinic [26].

Due to these excitation spectra results it is thus possible to choose the appropriate excitation wavelengths within the CT band to excite quasi-selectively ions located in different environments, either in regular sites of the cubic crystallites (at 250 nm excitation wavelength) or in perturbed sites of smaller and smaller nanometric cubic crystallites (at 270 and 290 nm excitation wavelength). This quasi-selective excitation may thus be considered as a size-selective excitation.

3.4.2. Composite films. Eu:Y_2O_3/Al_2O_3 composite films were analysed in the same way as the pure nanocrystalline Eu:Y_2O_3 films, by recording the emission spectra with the quasi-selective excitation in the CT band. The emission spectra of the film containing Eu:Y_2O_3 layers of 10 nm theoretical thickness are given in figure 8 for excitation wavelengths of 250, 270 and 290 nm. Although additional features similar to those observed for the nanocrystalline cubic Eu:Y_2O_3 film, as expected from the TEM observations, are present in these spectra, their contribution is larger. The main line at 611 nm, which is characteristic of ions in a well-defined C_2 site of the cubic cell, is predominant at 250 nm excitation, but is notably reduced at 270 nm excitation relative to the two lines located at 614.7 and 624 nm. At 290 nm excitation, only these two bands, strongly broadened, are detected. Whereas TEM observations show very well crystallized layers (figure 2), fluorescence spectroscopy emphasizes the presence of an enhanced contribution of perturbed sites, compared to pure nanocrystalline Eu:Y_2O_3 films, which should be attributed to sites with an increased disorder located at the interface with the alumina matrix.

For lower T_{theo}, the spectra are very weak and the main $^5D_0 \rightarrow {}^7F_2$ transition range is constituted by a single broad band between 610 and 630 nm, characteristic of an amorphous

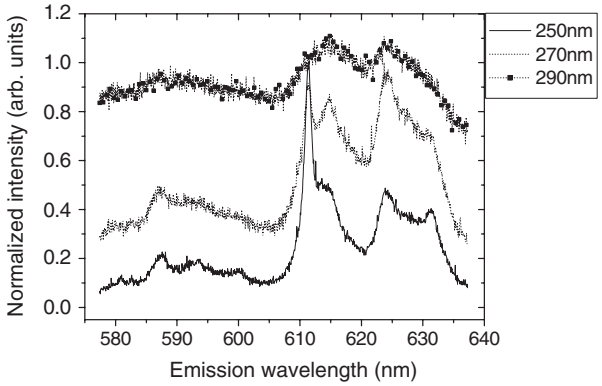

Figure 8. Emission spectra of composite Eu:Y_2O_3/Al_2O_3 films with 10 nm thick layers (λ_{exc} = 250, 270, 290 nm).

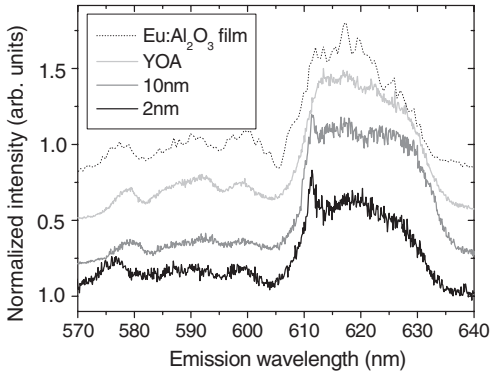

Figure 9. Emission spectra of composite Eu:Y_2O_3/Al_2O_3 films with 10 and 2 nm thick Y_2O_3 layers compared to YOA amorphous film and Eu:Al_2O_3 amorphous film [27] (λ_{exc} = 308 nm).

phase. In order to increase the signal, the emission spectra were registered under laser excitation at 308 nm. This wavelength corresponds to an excitation into the $^5F_2$ multiplet of the f configuration and into the low energy tail of the CT band, which should enhance the signal of perturbed ions. Figure 9 shows the emission spectra of films containing Eu:Y_2O_3 layers of theoretical thickness 10 and 2 nm. These spectra were registered with a delay of 300 μs, in order to eliminate a short-lived emission extending in the whole visible range and which had been attributed to the Al_2O_3 matrix by comparison with a pure alumina film. Whereas the $^5D_0 \rightarrow {}^7F_2$ spectrum for T_{theo} = 10 nm is characterized by the two broad lines located at about 615 and 624 nm already observed in figure 8(c), for T_{theo} = 2 nm the spectrum shows a broad band peaking at 620 nm. In addition, the $^5D_0 \rightarrow {}^7F_0$ line is enhanced and shifted from 580 to 575 nm. All the films with Eu:Y_2O_3 layer thickness equal to or less than 2 nm have similar spectra. The emission is thus mainly due to ions located in an amorphous phase or in sites of lower symmetry and disordered environment, in agreement with the TEM results. A comparison with the spectrum of an amorphous Eu:Y_2O_3 film, deposited at room temperature, shows that the $^5D_0 \rightarrow {}^7F_{0,2}$ lines of nanocomposite films are shifted relative to those of the amorphous Eu:Y_2O_3 film. The position of the lines roughly corresponds to those of Eu^{3+} emission in Al_2O_3 amorphous films [27]. As the theoretical thickness of the Y_2O_3 layers

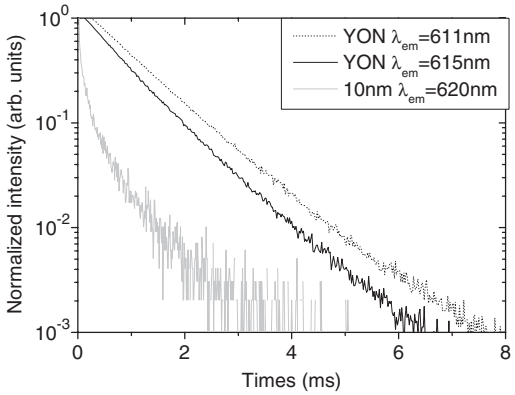

Figure 10. Fluorescence decays of the Eu:Y_2O_3 nanocrystalline film YON and Eu:Y_2O_3/Al_2O_3 composite film with 10 nm thick layers ($\lambda_{exc} = 308$ nm).

decreases, the contribution of the Al_2O_3/Y_2O_3 interfaces increases and provides an increase in the intensities of both the 620 nm broad band and the blue-shifted 575 nm $^5D_0 \rightarrow {}^7F_0$ line.

It should be noticed, however, that, for the composite films with layer thicknesses less than 2 nm, the narrow line located at 611 nm, which is characteristic of the C_2 site of the cubic phase, is detected even though these films are amorphous, according to TEM observations. This indicates that some Eu^{3+} ions are located in the few larger crystallites, which was evidenced in the size distribution of the nanoparticles by AFM, and may be crystalline, although not detected by TEM for which a smaller area is analysed. This could also be due to Eu^{3+} ions with a very local well-defined C_2 site environment, which play the role of nucleation centres and favour the layer crystallization induced by the electron beam in the microscope.

The influence of the alumina matrix may be further evidenced by the comparison of the fluorescence decay of pure and nanocomposite films, which are presented in figure 10. For the nanocrystalline YON film, the additional lines at 614 and 625 nm have identical decays, less exponential and faster than that of the 611 nm emission, which corresponds to the regular cubic sites and for which a mean 1 ms lifetime is measured. A similar shortening of the decay time of the perturbed ions, relative to the regular ones, has already been observed for nanocrystalline powders [28]. For the nanocomposite film with the 10 nm thick crystalline layers, the decay is strongly non-exponential and much faster. It does not depend significantly on the emission wavelength within the $^5D_0 \rightarrow {}^7F_2$ broad line because of the dominant contribution of the ions located in the perturbed sites at the Al_2O_3/Y_2O_3 interface, which, for the 308 nm excitation, are preferentially excited by comparison with those located in the core of the cubic crystallites. Very similar decays are observed for the broad band emission at 620 nm in the case of layers of 2 nm thickness and less.

Our fluorescence results agree with those reported for thin epitaxial Eu:Y_2O_3 layers deposited on α-Al_2O_3 [29], which emphasize the strong contribution of the interface sites. The same additional features, due to perturbed sites at the crystallite surface, are observed for 4 nm thick layers, although with a different relative contribution which may be due to the different excitation wavelengths. The same amorphous like spectrum is observed for thinner (1 nm) layers, which is attributed to the yttria/alumina interface. We also observed such an amorphous spectrum for single Eu:Y_2O_3 layers on alumina and composite multilayer films prepared at higher temperature (730 °C) and lower pressure (10^{-2} Pa), even for 20 nm thick layers. This dominant contribution of the perturbed interface sites was attributed to implantation or

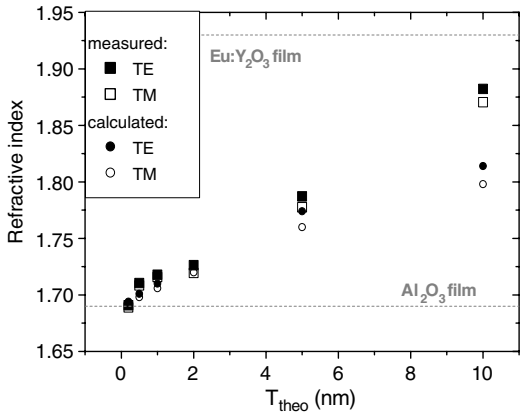

Figure 11. Refractive index at 543.5 nm of composite films as a function of the theoretical thickness of Eu:Y_2O_3 layers measured by m-line spectroscopy and calculated using the model of van der Ziel for transverse electric (TE) and transverse magnetic (TM) modes.

interdiffusion effects. They could not have been detected for the corresponding 800 nm thick Eu:Y_2O_3 film YOC (figure 7) because of the weak relative contribution of the interface layer in that case. Owing to the Eu^{3+} fluorescence, it is thus possible to get information on the structure of multilayers prepared with other deposition conditions by comparison of their fluorescence properties with those of the previously described multilayers, whose structural properties are known from TEM and AFM experiments.

3.5. Optical properties of the nanocomposite films

The refractive index and thickness of the composite films were measured by m-line spectroscopy at 543.5 nm. According to the expected refractive index range, 80 bilayers were deposited on silica substrates in order to provide multimode waveguides. As the theoretical thickness of Eu:Y_2O_3 layers increases, the refractive index, reported in figure 11, increases, due to the Eu:Y_2O_3 contribution, between the index of amorphous alumina ($n_{Al_2O_3} = 1.69$) and that of cubic Eu:Y_2O_3 ($n_{Y_2O_3} = 1.93$). An average refractive index was calculated as a function of the Eu:Y_2O_3 layer thickness ($T_{Y_2O_3}$), using the model of van der Ziel for multilayers [30]:

$$n_{TE}^2 = \frac{n_{Al_2O_3}^2 \times T_{Al_2O_3} + n_{Y_2O_3}^2 \times T_{Y_2O_3}}{T_{Al_2O_3} + T_{Y_2O_3}} \qquad n_{TM}^2 = \frac{T_{Al_2O_3} - T_{Y_2O_3}}{\frac{T_{Al_2O_3}}{n_{Al_2O_3}^2} + \frac{T_{Y_2O_3}}{n_{Y_2O_3}^2}}.$$

Due to the layered structure, the refractive indices for the TE mode (E parallel to the layer) and the TM mode (H parallel to layer) are different, although Al_2O_3 and cubic Y_2O_3 are not birefringent. This anisotropy is indeed observed especially for the 5 and 10 nm thick layers. For the thinnest Eu:Y_2O_3 layers ($T_{theo} < 2$ nm), which are amorphous according to the previous sections, this calculation was achieved using the refractive index of an amorphous Eu:Y_2O_3 film deposited at room temperature (1.90). The model agrees only moderately with the experimental values. The agreement could probably be improved using the Bragg–Pippard model for oriented ellipsoids [31] to take into account the fact that the layers contain isolated nanoparticles, if their extent were known. The strong increase of the refractive index for effective thicknesses of 5 and 10 nm is due to the crystallization of the Y_2O_3 nanolayers, because their refractive index is higher for the cubic phase than for the amorphous phase. The experimental values are, however, larger than expected from the model (figure 11). Within this

model, the refractive index to be taken into account for the layers should be notably higher than that of bulk cubic Y_2O_3, which should indicate modified polarizabilities for the nanocrystals, due to the complex interfaces evidenced by fluorescence.

Waveguiding propagation was observed for composite films with an effective thickness of 1 nm and less; the propagation losses were estimated to some dB cm^{-1} from the attenuation of the scattered light along the propagation line. This is more than those of alumina without nanolayers (<2 dB cm^{-1}) [16]. When the effective thickness increases further and crystallization takes place, an alteration of the optical waveguide quality was observed, which is indicated by a broadening of the dark lines, especially for TE polarization, and high scattering. No waveguiding propagation could then be detected.

4. Conclusion

Composite optical waveguides of Eu doped Y_2O_3 nanolayers embedded in an amorphous alumina matrix were prepared by pulsed laser deposition, with alternating ablation of two targets, in order to analyse the influence of the Eu:Y_2O_3 layer thickness (from 10 to 0.2 nm) on their structure and fluorescence properties. Deposition parameters (1 Pa oxygen pressure, 560 °C substrate temperature and 1 J cm^{-2} laser fluence) appropriate for growing amorphous alumina and Eu:Y_2O_3 nanocrystals, and the ablation pulse numbers on alumina and yttria targets necessary to adjust the deposited thickness (22 and 20 pulses nm^{-1} respectively), were determined from alumina and Eu:Y_2O_3 thick film deposition. Structure and fluorescence properties of Eu:Y_2O_3 layers on the alumina surface or in composites films were compared to those of thick amorphous, cubic or monoclinic Eu:Y_2O_3 films. They are strongly influenced by the theoretical thickness T_{theo} of the Eu:Y_2O_3 layers, the 10 nm thick alumina layer being amorphous. They show that Eu^{3+} ions in the composite films are distributed in different sites depending on the layer thickness.

For $T_{theo} \geqslant 5$ nm, smooth and continuous layers of (111) oriented cubic columnar nanocrystals are grown, as determined by TEM and AFM. The emission spectra are constituted by the superposition of different contributions, which can be excited quasi-selectively by scanning the excitation wavelength within the CTB, which appears as red-shifted when perturbed sites of smaller nanocrystal surfaces are considered. Eu^{3+} ions are located in regular sites of the cubic phase and in perturbed sites, attributed respectively to the crystallites core and surface, as has also been observed for nanocrystalline Eu:Y_2O_3 films. In addition, another kind of perturbed site is present. Its spectral and dynamic properties are characteristic of ions located in a strongly disordered phase and may be related to the interface with the amorphous alumina matrix.

For $T_{theo} \leqslant 2$ nm, the Eu:Y_2O_3 layers appear on TEM images as amorphous, rough and thicker than expected. AFM images of single layers show that they are constituted of isolated nanoparticles with heights mainly around 1 to 2 nm. The broad emission spectrum, characteristic of Eu^{3+} ions in an amorphous phase, appears similar to that of Eu^{3+} in alumina, which emphasizes the dominant role of the alumina/yttria interface. The presence of the 611 nm line, characteristic of Eu^{3+} ions with a regular cubic environment, in the spectra of Y_2O_3 layers with T_{theo} as low as 0.2 nm, may probably be explained by the polydispersity of the nanoparticle size distribution or indicate that the crystallization of the cubic phase, easily induced inside the electron microscope, begins around the Eu^{3+} ions.

The refractive index of the composite films, measured by m-line spectroscopy, increases as a function of the increasing yttria contribution and shows an increasing anisotropy, which is explained qualitatively by the layered structure of the films.

Optical waveguiding was obtained for the composites films with the thinnest Eu:Y_2O_3 layers but seems to be hindered by the layer crystallization.

PLD thus appears to be an efficient method for growing composite films containing crystalline or amorphous Eu:Y_2O_3 nanostructures in a single-step process without post-deposition treatment. Moreover this method prevents any surface contamination of the nanocrystals, as the deposition is achieved in a UHV chamber and they are embedded in an amorphous matrix without any contact with the air. Furthermore, experiments are under way to take advantage of the possibility provided by PLD to prepare nanocrystals by condensation within the plume at high pressure, rather than by crystallization on the substrate.

Acknowledgments

This research was supported by the European Community through a Marie Curie Individual Fellowship no HP MF-CT-2001-01492 (JL).

References

[1] Bihari B, Eilers H and Tissue B M 1997 *J. Lumin.* **75** 1
[2] Zhang W W, Zhang W P, Xie P B, Yin M, Chen H T, Jing L, Zhang Y S, Lou L R and Xia S D 2003 *J. Colloid Interface Sci.* **262** 588
[3] Strek W, Zych E and Hreniak D 2002 *J. Alloys Compounds* **344** 332
[4] Mercier B, Dujardin C, Ledoux G, Louis C, Tillement O and Perriat P 2004 *J. Appl. Phys.* **96** 650
[5] Bazzi R, Flores M A, Louis C, Lebbou K, Zhang W, Dujardin C, Roux S, Mercier B, Ledoux G, Bernstein E, Perriat P and Tillement O 2004 *J. Colloid Interface Sci.* **273** 191
[6] Flores-Gonzalez M A, Ledoux G, Roux S, Lebbou K, Perriat P and Tillement O 2005 *J. Solid State Chem.* **178** 989
[7] Wu Y C 2005 *PhD Thesis* University Lyon 1, France
[8] Korzenski M B, Lecoeur Ph, Mercey B, Camy P and Doualan J L 2001 *Appl. Phys. Lett.* **78** 1210
[9] Kumar D, Cho K G, Chen Z, Cracium V, Holloway P H and Singh R K 1999 *Phys. Rev.* B **60** 13331
[10] Lancok J, Garapon C, Martinet C, Mugnier J and Brenier R 2004 *Appl. Phys.* A **79** 1263
[11] Katiyar P, Kumar D, Nath T K, Kvit A V, Narayan J, Chattopadhyay S, Gilmore W M, Coleman S, Lee C B, Sankar J and Singh R K 2001 *Appl. Phys. Lett.* **79** 1327
[12] Serna R, Afonso C N, Ballesteros J M, Naudon A, Babonneau D and Petford-Long A K 1999 *Appl. Surf. Sci.* **138/139** 1
[13] Guinier A 1956 *Théorie et technique de la radiocristallographie* (Paris: Dunod)
[14] Ulrich R and Torge R 1973 *Appl. Opt.* **12** 2901
[15] Himel M D and Gibson U J 1986 *Appl. Opt.* **25** 4413
[16] Pillonnet A, Garapon C, Champeaux C, Bovier C, Brenier R, Jaffrezic H and Mugnier J 1999 *Appl. Phys.* A **69** S735
[17] Burmester P B W, Huber G, Kurfiss M and Schilling M 2003 *Appl. Phys.* A **80** 627
[18] Chang N C and Gruber J B 1964 *J. Chem. Phys.* **41** 3227
[19] Leavitt R P, Gruber J B, Chang N C and Morrison C A 1982 *J. Chem. Phys.* **76** 4775
[20] Forest H and Ban G 1969 *J. Electrochem. Soc.* **116** 474
[21] Qi Z M, Shi C S, Zhang W W, Zhang W P and Hu T D 2002 *Appl. Phys. Lett.* **81** 2857
[22] Masenelli B, Mélinon P, Nicolas D, Bernstein E, Prével B, Kapsa J, Boisron O, Perez A, Ledoux G, Mercier B, Dujardin C, Pellarin M and Broyer M 2005 *Eur. Phys. J.* D **34** 139
[23] Williams D K, Bihari B, Tissue B M and McHale J M 1998 *J. Phys. Chem.* B **102** 916
[24] Skandan G, Forster C M, Frase H, Ali M N, Parker J C and Hahn H 1992 *Nanostruct. Mater.* **1** 313
[25] Tissue B M and Yuan H B 2003 *J. Solid State Chem.* **171** 12
[26] Hoefdraad H E 1975 *J. Solid State Chem.* **15** 175
[27] Minardi A, Garapon C, Mugnier J and Champeaux C 2001 *Mater. Res. Soc. Symp. Proc.* **667** G3.10
[28] Zhang W W, Xu M, Zhang W, Yin M, Qi Z, Xia S and Garapon C 2003 *Chem. Phys. Lett.* **376** 318
[29] Burmester P B W, Ishii T, Huber G, Kurfiss M and Schilling M 2003 *Mater. Sci. Eng.* B **105** 25
[30] Van der Ziel J P 1975 *Appl. Phys. Lett.* **26** 60
[31] Bragg W L and Pippard A B 1953 *Acta Crystallogr.* **6** 865